Available online at www.sciencedirect.com

ScienceDirect

Acta Materialia 81 (2014) 211–218

Acta MATERIALIA

www.elsevier.com/locate/actamat

Multiscale mechanics to determine nanocomposite elastic properties with piezospectroscopy

Gregory Freihofer [a], Axel Schülzgen [b], Seetha Raghavan [a,*]

[a] Mechanical and Aerospace Engineering Department, University of Central Florida, 4000 Central Florida Blvd., Orlando, FL 32816, USA
[b] CREOL, The College of Optics and Photonics, University of Central Florida, 4000 Central Florida Blvd., Orlando, FL 32816, USA

Received 26 June 2014; received in revised form 30 July 2014; accepted 1 August 2014

Abstract

The piezospectroscopic (PS) properties of chromium-doped alumina allow for embedded inclusion mechanics to be revisited with unique experimental setups that probe the particles' state of stress when the composite is under applied load. These experimental investigations of particle mechanics will be compared to the Eshelby theory and a derivative theory. This work discovers that simple nanoparticle load transfer theories are adequate for predicting PS properties in the low to intermediate volume fraction range ($\leqslant$20%). By applying the multiscale mechanics to a PS response, the inverse problem was demonstrated to reveal the elastic modulus of the composite. The implications for this technique are damage monitoring through observation of reduced mechanical properties in addition to a method to assist with engineering nanomaterials.

Keywords: Particulate mechanics; Piezospectroscopy; Alumina; Load transfer

1. Introduction

Piezospectroscopy is a technique to measure stress using the spectral emissions of a material. This has been commonly applied to ruby as pressure sensors for diamond anvil cells [1], and indicators of residual stress build up in the alumina oxide layer of thermal barrier coatings [2]. Recent efforts that introduced photoluminescent alumina nanoparticles as a constituent into a matrix material have shown them to enhance the stress sensitivity of the resulting nanocomposite [3]. Such non-invasive measurements of microscale stresses with multiscale spatial resolution assist in the engineering of advanced nanocomposites. Although such PS measurements are only possible when there are embedded inclusions which exhibit intrinsic PS properties, the insights gained from measurements using these materials can be used to obtain a greater understanding of particulate composites mechanics. Similar works studied the strength of alumina and sapphire fiber bundles by quantifying the volume of damaged to undamaged fibers using piezospectroscopy [4]. Here, a unique combination of piezospectroscopic (PS) and particulate mechanics is presented that enables the determination of nanocomposite elastic properties.

Particulate nanocomposites have shown great promise for future applications because the intrinsic size effect produces enhanced mechanical properties [5]. One of the many types of nano- or microinclusions that have been used in developing nanocomposites is ceramic particles such as alumina, which has high hardness and excellent retention of strength at high temperatures [6]. The trace amounts of Cr^{3+} impurities in alumina afford excellent PS properties [7]. In general, when the particles are added to a matrix they increase the fracture toughness, wear resistance and elastic modulus with respect to unfilled matrix. However, there are many microstructural factors

* Corresponding author.

http://dx.doi.org/10.1016/j.actamat.2014.08.003
1359-6454/

to consider when evaluating the performance. These factors include particle size [8–11], particle shape [12,13], surface treatment [11,12,14,15] and dispersion [9]. These factors are not limited just to alumina composites but also apply to particulate composites in general.

The application of piezospectroscopy could supply an enhanced understanding of the micromechanics of particulate composites. The ability to experimentally probe the stresses and strains of the particle phases has been limited to less accessible high energy X-ray [16] and neutron [17] diffraction techniques. Therefore, much of the design of these composites depend on the bulk strain response of the composite from strain gage or computational simulations of the nanocomposite. Previous results have shown that the complex micromechanics of alumina plasma-spray coatings under in situ mechanical loading was revealed with piezospectroscopy in great detail when compared to a conventional bulk strain measurement [18]. In addition, piezospectroscopy can point out micron-level structural defects in such materials with its capability of high spatial resolution [19].

This investigation begins with an effort to analytically replicate the experimental PS coefficients of alumina–epoxy nanocomposites from a combination of previous works [3,20] where increasing the volume fraction of alumina resulted in enhanced sensitivity of the PS properties. The state of stress obtained by the PS measurements will be discussed along with the approach of comparing it with theoretical calculations. A generalized method of calculating stresses of the embedded inclusions will be presented which was inspired by the works of Kim [21]. Then the application of multiscale mechanics will be shown to convert nanoparticle stresses from piezospectroscopy into elastic property calculations of the bulk composite.

2. Experimental background

When under compressive load, the spectral emissions of the Cr^{3+} doped polycrystalline alumina have been shown to exhibit negative wavenumber shifts [7,22]. This trend is also observed when the alumina is distributed as nanoparticles within an epoxy matrix, as illustrated in Fig. 1a and b. The rate of this wavenumber shift is much higher for the nanocomposites, indicating increased PS sensitivity. This was quantified directly by the experimental works of Stevenson [3], and then later it was substantiated by testing additional volume fractions [20]. The PS sensitivity of the composite can be quantified by the PS coefficient (Π_c) and defined as the rate of PS shift per applied uniaxial external stress to the composite, as illustrated in Fig. 1c.

The PS coefficient for bulk polycrystalline alumina under uniaxial compression has been recorded to be 2.54 cm^{-1}/GPa [7]. Recent work has established the PS coefficients for alumina–epoxy nanocomposites for different volume fractions of alumina, and these are shown in Table 1 [3,20]. The experiments were conducted with alumina nanoparticles (150 nm) embedded in an EPON 826 epoxy matrix. The samples were manufactured as parallelepipeds, using ASTM standard D695 [23].

The wavenumber shifts of the PS response are usually very small ($\leq 1 cm^{-1}$) for conventional mechanical tests. However, pseudo-Voigt curve-fitting algorithms can resolve even smaller changes in peak position with a standard deviation less than 0.01 cm^{-1} [3,24]. A systematic uncertainty with a stress measurement of 200 MPa gives an error of 0.05 cm^{-1}/GPa for the composite PS coefficients in Table 1. Details on the experimental setup used to obtain results in Table 1 are found elsewhere [25].

Table 1
Experimental PS coefficients (Π_c) for R1 and R2 peaks [3,20].

Volume fraction %	R1 cm^{-1}/GPa	R2 cm^{-1}/GPa
5	−3.16	−2.60
20	−3.34	−3.19
25	−3.65	−3.42
34	−4.10	−3.88
38	−5.63	−5.08

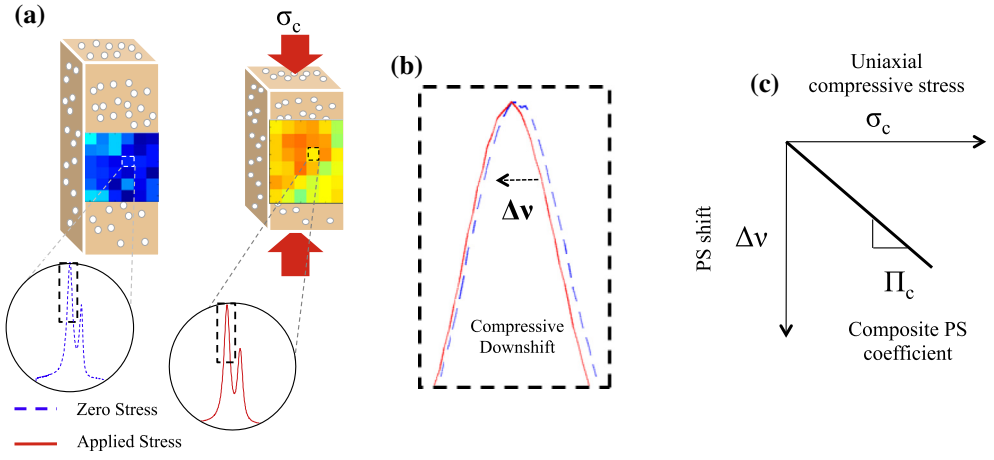

Fig. 1. (a) A schematic representing hyperspectral imaging of a PS nanocomposite under compressive loading, (b) the corresponding peak position downshifts with compressive loading and (c) the composite PS coefficient (Π_c) relating a peak position shift with applied stress.

3. Piezospectroscopic nanocomposite mechanics

Here, the PS relationships are explored to establish how they can be integrated with inclusion mechanics. The PS shifts of the photoluminescent (PL) R-lines for polycrystalline Cr-doped alumina (Δv) have been correlated in the literature to the first stress invariant σ_{ii} by the PS coefficient $\frac{1}{3}\Pi_{ii}$ in Eq. (1) [7]. For the stress sensitive peaks, Π_{ii} has a value of 7.59 and 7.62 cm^{-1}/GPa for R1 and R2 in polycrystalline alumina respectively [7]. When uniaxial stress (σ_a) is applied to an alumina polycrystal, Eq. (1) will give a PS coefficient of 2.54 cm^{-1}/GPa and the response is illustrated in Fig. 2:

$$\Delta v = \frac{1}{3}\Pi_{ii}\sigma_{ii} \tag{1}$$

When an embedded polycrystalline alumina particle is within a matrix and uniaxial stress (σ_a) is applied to the composite, the inclusion mechanics create an equibiaxial state of stress on the inclusion. Because the alumina nanocomposite's PS coefficients (Π_c) are larger than bulk alumina polycrystal, as observed in Table 1, this leads to the conclusion that the first invariant of stress is also larger for the embedded particle than its bulk counterpart. If the uniaxial stress σ_a was applied as pressure to the particle on all principal axes, then the observed PS coefficient would be even greater than all of the observed uniaxial PS coefficients for the nanocomposites, as illustrated in Fig. 2.

It is noteworthy that all the Π_c values fall between Π_{ii} and $\frac{\Pi_{ii}}{3}$. It is hypothesized that these values may act as upper and lower limits for Π_c because they represent idealized configurations.

The PS shift of an alumina–epoxy nanocomposite is shown in Eq. (2). To understand the relationships between the nanocomposite response with the ideal configurations of the bulk counterpart, Eqs. (1) and (2) are incorporated into Eq. (3):

$$\Delta v = \Pi_c \sigma_a \tag{2}$$

$$\frac{\frac{1}{3}\sigma_{ii}}{\sigma_a} = \frac{\Pi_c}{\Pi_{ii}} \tag{3}$$

Eq. (3) is an important expression that reveals a direct measure of the first invariant of the particle with the experimental PS coefficient. The left-hand side can be used to correlate theoretical models to experimentally measured PS coefficients on the right-hand side. The left-hand side, which is the rate of hydrostatic stress induced on the particle per uniaxial stress on the composite, will henceforth be termed the stress ratio.

3.1. Analytical formulation

The stress ratio defined in the previous section can be predicted using inclusion mechanics, which determines the stress in the particle through analytical or numerical techniques. Here, the classical Eshelby model for dilute systems [26] was used to estimate the stress ratio. The Eshelby model used here has several assumptions, as follows: (i) a single particle is embedded in an infinite matrix (infinitesimal volume fraction); (ii) the nanoparticle is perfectly spherical; (iii) perfect bonding occurs between the nanoparticle and the matrix; and (iv) both the nanoparticle and the matrix phase are isotropic. This basic model, despite its many assumptions, was shown in previous work to be closely correlated to the experimental data obtained for the lowest volume fraction of 5% [27].

The formulation [28] is based on a spherical particle (p) embedded within an isotropic matrix (m). The stress inside the particle (σ^p) can be calculated from multiple strain terms shown in Eqs. (4)–(6), where e, e^o and e^* represent the strain disturbed by the filler, the mechanical strain of the matrix from applied load and the equivalent eigenstrain of the inclusion problem, respectively. Additionally, C and S represent the stiffness and Eshelby tensors, respectively [28].

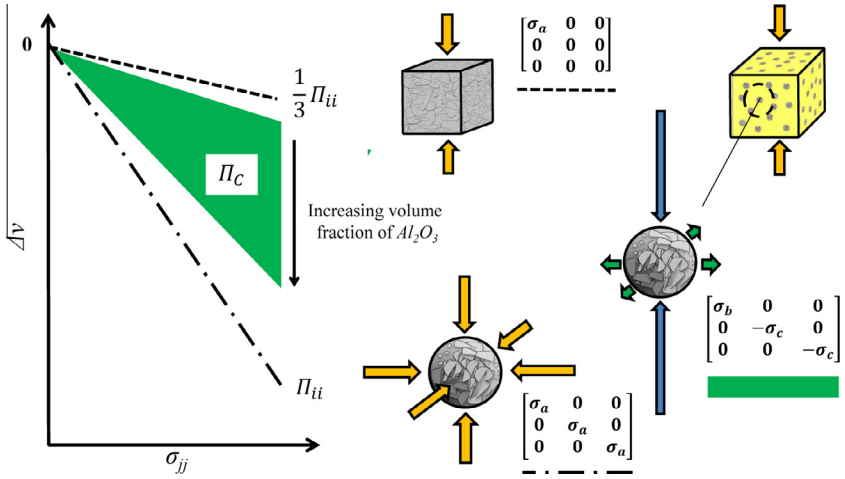

Fig. 2. The Piezospectroscopic relationships for different loading conditions of a PS constituent.

$$e = Se^* \tag{4}$$

$$e^o = (C^m)^{-1}\sigma^m \tag{5}$$

$$e^* = -[(C^p - C^m)S + C^m]^{-1}(C^p - C^m)(C^m)^{-1}\sigma^m \tag{6}$$

Finally, by using the above strain terms, the stress inside the filler can be computed from the applied stress to the matrix using Eq. (7) [28]:

$$\sigma^p = C^m(e^o + e - e^*) \tag{7}$$

From here, the dilute Eshelby equations from the literature [28] were modified for correlation with piezospectroscopy. The first step is to combine the three different components of strain into Eq. (7). Then, with the application of Hooke's law, the expression can be rearranged to relate the strain tensors between the particle and matrix in Eq. (8) by a fourth-order tensor F in Eq. (9):

$$F\epsilon^m = \epsilon^p \tag{8}$$

$$F = (C^p)^{-1}C^m[I - (S - I)[(C^p - C^m)S + C^m]^{-1}(C^p - C^m)] \tag{9}$$

This simplified relationship can be viewed in Voigt notation in Eq. (10). The scalar components that make up the fourth-order tensor F can be shown to relate the first strain invariants between the particle and composite phases in Eq. (11), and is a function of the elastic properties of both matrix and particle in Eq. (12). Since the first invariant of stress and strain are proportional by the bulk modulus ($\sigma_{ii} = 3K\epsilon_{ii}$), a similar expression can be shown to relate the first stress invariants of the two particles in Eq. (13) to give the stress ratio:

$$F = \begin{vmatrix} F_1 & F_2 & F_2 & 0 & 0 & 0 \\ F_2 & F_1 & F_2 & 0 & 0 & 0 \\ F_2 & F_2 & F_1 & 0 & 0 & 0 \\ 0 & 0 & 0 & F_3 & 0 & 0 \\ 0 & 0 & 0 & 0 & F_3 & 0 \\ 0 & 0 & 0 & 0 & 0 & F_3 \end{vmatrix} \tag{10}$$

$$(F_1 + 2F_2)\epsilon^m_{ii} = \epsilon^p_{ii} \tag{11}$$

$$\frac{\epsilon^p_{ii}}{\epsilon^m_{ii}} = \frac{-3E^m(2\nu^p - 1)(\nu^m - 1)}{(2\nu^m - 1)(2E^m + E^p - 4E^m\nu^p + E^p\nu^m)} \tag{12}$$

$$\frac{\sigma^p_{ii}}{\sigma^m_{ii}} = \frac{-3E^p(\nu^m - 1)}{2E^m + E^p - 4E^m\nu^p + E^p\nu^m} \tag{13}$$

It is noteworthy that both expressions are functions of material properties of the host matrix and embedded particles. The stress-based expression in Eq. (13) will be used to simulate the effects of volume fraction for comparison to the experimental PS coefficients from the works of Ergin [20] and Stevenson [3]. The strain based expression in Eq. (12) will be used to calculate material properties of an alumina–epoxy nanocomposite when the observed PS response is referenced to a secondary strain gage measurement.

4. Simulating volume fraction effects

The dilute Eshelby equations represent an infinitesimal volume fraction and will be used to estimate the PS coefficient of a composite. Using the material properties of the inclusion phase of α-Al_2O_3 ($E^p = 300$ GPa, $\nu^p = 0.2$) and an isotropic matrix phase of EPON 862 ($E^m = 2.41$ GPa, $\nu^m = 0.4$), the stress ratio can be calculated and compared to the experimental data. Using Eq. (3) and observing Fig. 3, the comparison shows that the Eshelby model accurately predicts the smaller volume fraction's stress ratio.

However, this dilute Eshelby model only takes into account an infinitesimal volume fraction because of the first assumption stated earlier. Eshelby modified his own dilute assumption for a non-dilute case. This non-dilute Eshelby model uses a different eigenstrain, which is now a function of volume fraction f in Eq. (14) [28]:

$$e^* = -[(C^m - C^p)(S - f(S - I) - C^m]^{-1}](C^m - C^p)(C^m)^{-1}\sigma^m \tag{14}$$

From inspection of Fig. 3, the non-dilute Eshelby diverges away from experimental data for higher volume

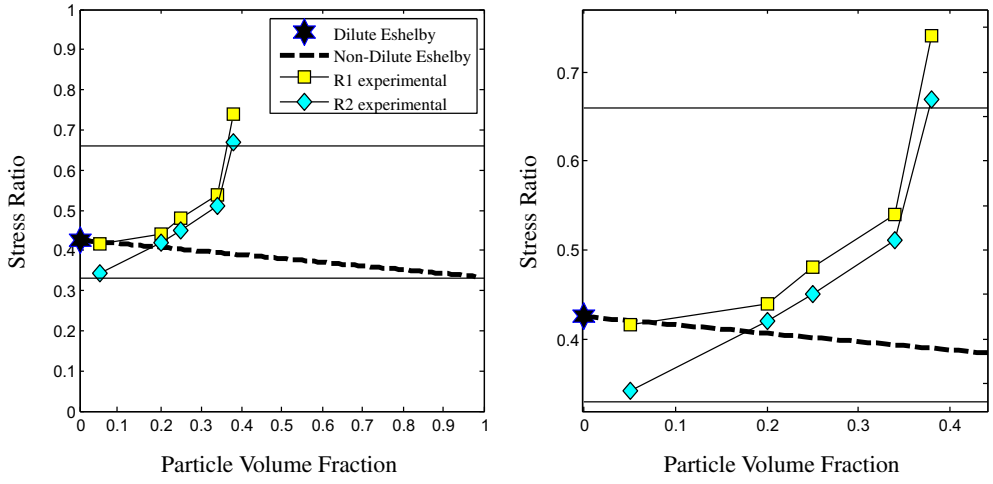

Fig. 3. The theoretical Eshelby [26,28] model predicting the PS properties for a composite and compared to experimental data from the works of Ergin [20] and Stevenson [3].

fractions. It is observed that the predicted stress ratio of the non-dilute Eshelby model approaches $\frac{1}{3}$. This is because a bulk polycrystalline alumina under uniaxial stress would show a third as much PS sensitivity compared to when the pressure is applied in a hydrostatic fashion. This concept was previously illustrated in Fig. 2. Fig. 3 shows that the experimental stress ratios continue to increase with increasing volume fraction. This creates a motivation for adapting modified Eshelby solutions to more accurately predict the PS properties of composites for higher volume fractions.

There are many different models in the literature for estimating equivalent composite properties for varying volume fractions [29–34], but estimating the stress sustained by the particle requires an alternative approach. The goal is to use equivalent composite property models to better predict the PS properties for varying volume fraction. This was motivated by the work of Kim [21], who developed his own iterative technique to predict composite properties, but here it will be taken a step further by demonstrating that any equivalent composite property model can be applied to predict the stress of the embedded inclusion.

Kim et al. [21] created an iterative programming loop that adds infinitesimal volume fractions and iterates new equivalent matrix properties for increasing volume fractions. This technique is referred to as successive embedding. The framework of this technique is described in the literature [21]. It is based on an assumption that the Eshelby equations can be used with the matrix properties replaced by equivalent composite properties.

Here, Kim's successive embedding technique was recreated to obtain the stress ratio of the composite in order to predict the PS properties of the composite. The results are plotted with the experimental data in Fig. 5. The method was successful in predicting PS properties for low and intermediate volume fractions $\leqslant 20\%$ with good accuracy. At volume fraction of 38% alumina, the experimental results show a dramatic increase in the stress ratio that deviate from the current model.

To continue the development of these load transfer models, an alternative and more general method of modifying the Eshelby theory is proposed. This new method would be compatible with different prediction schemes, as shown in Fig. 4. A different equivalent composite property model could be treated as the new inputs for the dilute Eshelby equations.

The equivalent composite properties model chosen to demonstrate the method illustrated in Fig. 4 was the Mori–Tanaka method [35,36]. This model was chosen because it assumes that the composite is isotropic and contains randomly distributed spherical inclusions. The equations which govern this model are given below. K and G represent the bulk and shear moduli,respectively, of the matrix (m) and the particle (p), with a particle volume fraction f [35].

$$G^c = G^m + \frac{fG^m(G^p - G^m)}{G^m + \beta_1(1-f)(G^p - G^m)} \tag{15}$$

$$K^c = K^m + \frac{fK^m(K^p - K^m)}{K^m + \beta_2(1-f)(K^p - K^m)} \tag{16}$$

where

$$\beta_1 = \frac{2(4-5\nu^m)}{15(1-\nu^m)} \quad \text{and} \quad \beta_2 = 3 - 5\beta_1 \tag{17}$$

It is desired that the Elastic modulus and Poisson's ratio are the two independent properties which describe the isotropic properties of the composite because these are standard parameters from measurements performed in materials testing. This is done so by Eq. (18).

$$E^c = \frac{9K^cG^c}{3K^c + G^c} \qquad \nu^c = \frac{E^c}{2G^c - 1} \tag{18}$$

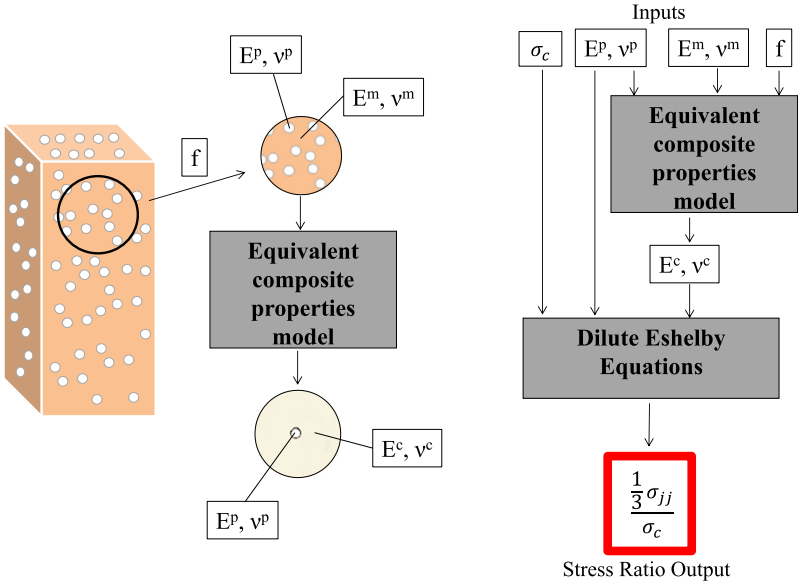

Fig. 4. A modified Esheby scheme which has the potential to combine any material properties prediction model for composites.

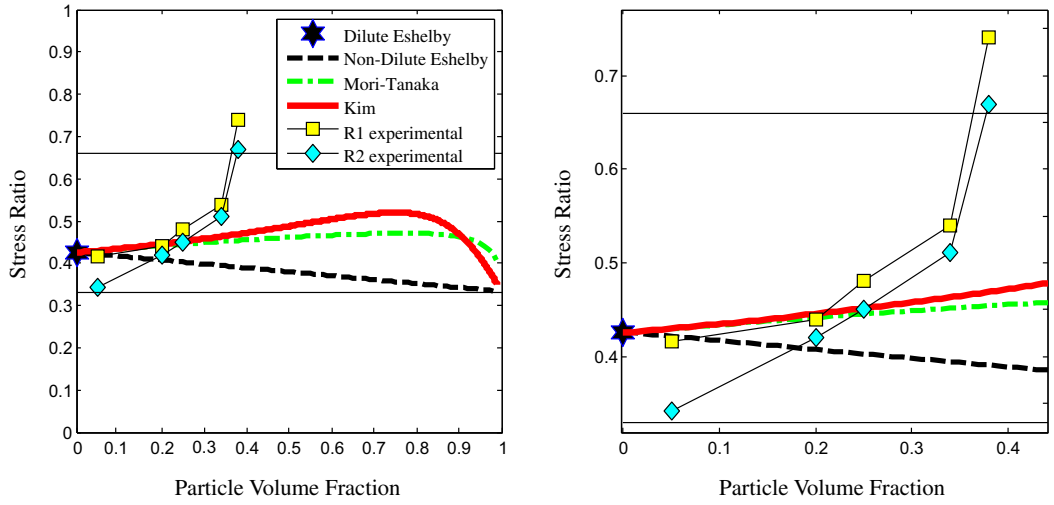

Fig. 5. The equivalent composite properties model utilizing the Mori–Tanaka equations [35] compared to Kim's method [21], non-dilute Eshelby [28], and experimental data from Ergin [20] and Stevenson [3].

Now, the Mori–Tanaka equivalent composite property model will be combined with the dilute Eshelby model using the process illustrated in Fig. 5. The results are very similar to the successive embedding method of Kim. The benefits of this general method are that it is flexible enough to apply a variety of different equivalent composite property models from the literature and also provides a direct approach to solving the stress ratio without an iterative solution.

From the current results shown in Fig. 5, all analytical models still underpredict the stress in the particles compared to what was experimentally observed for high volume fractions ($\geqslant$20%). The effect of microstructural features and contact stresses present at higher volume fractions could potentially contribute to this difference. Alternative methods to analytically predicting the stress in the nanoparticles are possible through finite element models (FEMs) [37–39]. By use of an FEM of the nanoparticle system, insights may be gained as to what specific microstructural feature leads to this dramatic increase in the stress ratio for higher volume fractions. Exploring these options and applying a wide variety of equivalent composite property models to the method proposed here provides room for future work.

5. The inverse problem

With the PS properties estimated using composite mechanics, the inverse solution will now take the PS response from a composite to infer the material properties of the bulk nanocomposite. A previous experiment conducted by Ergin [20] examined the intermediate to higher volume fraction range with 20%, 30% and 34% volume fraction alumina. This is the range of volume fractions where a large increase in PS sensitivity is expected to occur [3]. In addition to reporting the PS coefficients, Ergin also deployed strain gages to measure the elastic modulus of the nanocomposites. Therefore, the inverse problem was only applied to the three volume fractions with complementary strain gage data in order to compare the elastic modulus measured by conventional means.

When the PS shift is measured against a strain gage measurement (ϵ_1), the transformation between the two measurements can be shown to be a combination of ratios in Eq. (20). This relationship is usually defined as the composite's PS coefficient (Π_c).

$$\Delta v = \frac{\Delta v}{\epsilon_{ii}^p}\frac{\epsilon_{ii}^p}{\epsilon_{ii}^c}\frac{\epsilon_{ii}^c}{\epsilon_1^c}\epsilon_1^c = \Pi_c \epsilon_1^c \tag{19}$$

The first ratio describes the PS mechanics which can be obtained by converting the first stress invariant in Eq. (1) into the first strain invariant by the particle's bulk modulus (K^p).

$$\frac{\Delta v}{\epsilon_{ii}^p} = K^p \Pi_{ii} \tag{20}$$

The next ratio in the transformation is from the particle mechanics. In the previous section it was first shown that the PS coefficient is a function of material properties of the particle and host matrix, then it was demonstrated that the material properties of the matrix can be replaced by equivalent mechanical properties of the matrix for greater accuracy. Therefore, Eq. (12) can be rewritten as Eq. (21), which includes the nanocomposites mechanical properties:

$$\frac{\epsilon_{ii}^p}{\epsilon_{ii}^c} = \frac{-3E^c(2\nu^p-1)(\nu^c-1)}{(2\nu^c-1)(2E^c+E^p-4E^c\nu^p+E^p\nu^c)} \tag{21}$$

The last ratio is the transformation of the first strain invariant of the particle to the uniaxial strain measured by the strain gage. The samples were manufactured under ASTM standard D-695 for compression of rigid plastics [23], which conventionally assumes uniaxial stress. However, this assumption requires a prediction of the composite's Poisson's ratio (ν^c). An assumption of uniaxial strain enables the removal of the Poisson's effect and allows

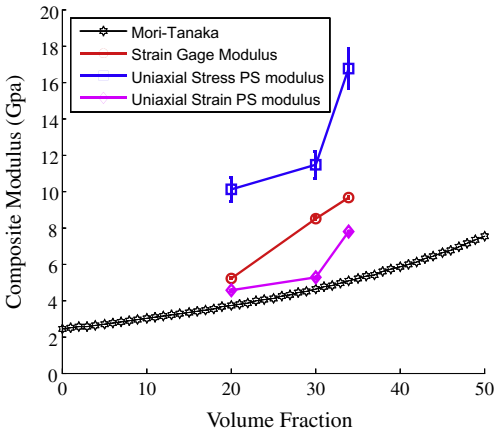

Fig. 6. Composite modulus based on the calculation of the PS response with uniaxial stress/strain, the load cell/strain gage response and the analytical Mori–Tanaka solution [36].

for an alternative expression. The last ratio under the assumptions of uniaxial stress and strain are shown separately in Eq. (22):

$$\frac{\epsilon^c_{ii}}{\epsilon^c_1} = 1 - 2\nu^c, \quad \frac{\epsilon^c_{ii}}{\epsilon^c_1} = 1 \tag{22}$$

The combined expression with all of the ratios is a function of the material properties for the equivalent bulk composite and the particle. The material properties of the particles are known and chosen to be identical to its bulk counterpart [6], which removes all the variables associated with the particle, including E^p, K^p, ν^p and Π_{ii}. The composite's PS coefficient Π_c is experimentally measured, which leaves only the equivalent composites material properties E^c and ν^c. Eq. (20) can be rearranged for a direct solution of the composites elastic modulus for the uniaxial stress and strain states in Eqs. (23) and (24), respectively:

$$E^c = \frac{-E^p\Pi_c(\nu^c + 1)}{[2\Pi_c + 3K^p\Pi_{ii}(1-\nu^c)](2\nu^p - 1)} \tag{23}$$

$$E^c = \frac{-E^p\Pi_c}{(2\Pi_c + 3K^p\Pi_{ii})(2\nu^p - 1)} \tag{24}$$

Both calculations of the composite's elastic modulus were performed and plotted in Fig. 6, along with the conventional strain gage load cell calculated modulus and also the prediction with the Mori–Tanaka method. For the uniaxial stress case, ν^c needs to be estimated, which introduces significant uncertainty because it was estimated using the Mori–Tanaka approach. With the multiscale mechanics applied to the PS response, calculations of material properties were obtained with good accuracy when compared to the conventional methods.

6. Conclusion

This work investigated PS properties of nancomposites. Inclusion mechanics based on the Eshelby theory proved to accurately predict the PS properties of nanocomposites for low volume fractions. A modification to the Eshelby model extended the prediction capabilities to intermediate volume fractions ($\leqslant$20%). This involved combining the dilute Eshelby equations with existing equivalent mechanical property models.

With the mechanics demonstrating the ability to predict PS properties, the inverse problem was solved. This included interpreting the PS response to infer the mechanical properties of the bulk composite. Equations were derived which showed the relationships between the elastic modulus and the observed PS response. The results showed that the elastic modulus of the composite calculated from the PS response agreed well with conventional methods, such as strain gage and load cell data.

The ability to obtain material properties from the PS response is a significant contribution to the field. The spatial capabilities with piezospectroscopy enables the detection of locally damaged regions which contain reduced material properties. Mapping local material properties has implications for damage assessment in materials and can assist in the design of advanced nanocomposites.

Acknowledgements

This material is based upon work supported by the National Science Foundation under Grant No. CMMI 1130837 and the University of Central Florida Office of Research and Commercialization Inhouse Grant FY 2012. Ms. Hong Tat from Boeing Research & Technology is acknowledged for technical discussions.

References

[1] Piermarini GJ, Block S, Barnett JD, Forman RA. Calibration of the pressure dependence of the R_1 ruby fluorescence line to 195 kbar. J Appl Phys 1975;46:2774.
[2] Selcuk A, Atkinson A. Analysis of the Cr^{3+} luminescence spectra from thermally grown oxide in thermal barrier coatings. Mater Sci Eng A 2002;A335:147–56.
[3] Stevenson A, Jones A, Raghavan S. Stress-sensing nanomaterial calibrated with photostimulated luminescence emission. Nano Lett 2011;11:3274.
[4] He J, Clarke D. Determination of fibre strength distributions from bundle tests using optical luminescence spectroscopy. Proc Roy Soc Lond. Ser A: Math Phys Eng Sci 1997;453(1964):1881–901.
[5] Zhu T, Bushby A, Dunstan D. Materials mechanical size effects: a review. Mater Sci Technol 2008;23(4):193–209.
[6] Munro RG. Evaluated material properties for a sintered α alumina. J Am Ceram Soc 1997;80:1919–28.
[7] He J, Clarke DR. Determination of the piezospectroscopic coefficients for chromium doped sapphire. J Am Ceram Soc 1995;78(5):1347–53.
[8] Marur P, Batra R, Garcia G, Loos A. Static and dynamic fracture toughness of epoxy/alumina composite with submicron inclusions. J Mater Sci 2004;39(4):1437–40.
[9] Zunjarrao SC, Singh RP. Characterization of the fracture behavior of epoxy reinforced with nanometer and micrometer sized aluminum particles. Compos Sci Technol 2006;66(13):2296–305.
[10] Cho J, Joshi M, Sun C. Effect of inclusion size on mechanical properties of polymeric composites with micro and nano particles. Compos Sci Technol 2006;66:1941–52.

[11] Douce J, Boilot J-P, Biteau J, Scodellaro L, Jimenez A. Effect of filler size and surface condition of nano-sized silica particles in polysiloxane coatings. Thin Solid Films 2004;466(1):114–22.
[12] Lim S, Zeng K, He C. Morphology, tensile and fracture characteristics of epoxy–alumina nanocomposites. Mater Sci Eng: A 2010;527(21):5670–6.
[13] Burris DL, Sawyer WG. Improved wear resistance in alumina-PTFE nanocomposites with irregular shaped nanoparticles. Wear 2006; 260(7):915–8.
[14] Ji QL, Zhang MQ, Rong MZ, Wetzel B, Friedrich K. Tribological properties of surface modified nano-alumina/epoxy composites. J Mater Sci 2004;39(21):6487–93.
[15] Shao X, Xue Q, Liu W, Teng M, Liu H, Tao X. Tribological behavior of micrometer- and nanometer-Al_2O_3-particle-filled poly (phthalazine ether sulfone ketone) copolymer composites used as frictional materials. J Appl Polym Sci 2005;95(5):993–1001.
[16] Roy S, Gibmeier J, Kostov V, André K. Internal load transfer and damage evolution in a 3D interpenetrating metal/ceramic composite. Mater Sci Eng 2012;A551:272–9.
[17] Winand H, WHitehouse A, WIthers P. An investigation of the isothermal creep response of AL-based composites by neutron diffraction. Mater Sci Eng 2000;A284:103–13.
[18] Freihofer G, Fugon-Dessources D, Ergin E, Newkirk AV, Gupta A, Seal S, et al. Piezospectroscopic measurements capturing the evolution of plasma spray-coating stresses with substrate loads. Appl Mater Interfaces 2014;6(3):1366–9.
[19] Freihofer G, Gupta A, Newkirk AV, Seal S, Raghavan S. Optical stress sensing alumina nanocomposite coatings for aerospace structures. In: AIAA SciTech, 55th AIAA/ASME/ASCE/AHS/SC structures, structural dynamics, and materials conference, 2014.
[20] Ergin E. Development of nanoparticle piezospectroscopy for in situ health monitoring. Master's thesis, Chalmers University of Technology; 2012.
[21] Kim J, Lee J. A new model to predict effective elastic constants of composites with spherical fillers. J Mech Sci Technol 2006;20:1891–7.
[22] Grabner L. Spectroscopic technique for the measurement of residual stress in sintered Al_2O_3. J Appl Phys 1978;49(5):580–3.
[23] ASTM. Standard test method for compressive properties of rigid plastics D-695 (02a). Tech. rep., American Society for Testing and Materials; 2002.
[24] Raghavan S, Imbrie P, Crossley WA. The spectral analysis of R lines and vibronic sidebands in the emission spectrum of ruby using genetic algorithms. Appl Spectrosc 2008;62:759–65.
[25] Freihofer G, Poliah L, Walker K, Medina A, Raghavan S. Optical stress probe: in situ stress mapping with raman and photo-stimulated luminescence spectroscopy. J Instrum 2010;5:P12003.
[26] Eshelby R. The determination of the elastic field of an ellipsoidal inclusion, and related problems. Proc Roy Soc Lond 1957;A241: 376–96.
[27] Freihofer GJ, Frank S, Ergin E, Jones AS, Stevenson A, Schülzgen A, et al. Measurement of load transfer within alumina nanoparticle epoxy composites using piezospectroscopy. In: Proceeding of the society for the advancement of material and process engineering 2012 conference, 21–24 May 2012, Baltimore (MD); 2012.
[28] Clyne T, Withers P. An introduction to metal matrix composites. Press Syndicate of the University of Cambridge; 1993.
[29] Duan H, Yi X, Huang Z, Wang J. A unified scheme for prediction of effective moduli of multiphase composites with interface effects. Part I: Theoretical framework. Mech Mater 2007;39:81–93.
[30] Wu YM, Huang Z, Zhong Y, Wang J. Effective moduli of particle-filled composite with inhomogeneous interphase: Part i – Bounds. Compos Sci Technol 2004;64:1345–51.
[31] Benabou L, Naït Abdelaziz M, Benseddiq N. Effective properties of a composite with imperfectly bonded interface. Theor Appl Fract Mech 2004;41(1):15–20.
[32] Zimmerman RW. Elastic moduli of a solid containing spherical inclusions. Mech Mater 1991;12(1):17–24.
[33] Lewis T, Nielsen L. Dynamic mechanical properties of particulate-filled composites. J Appl Polym Sci 1970;14(6):1449–71.
[34] Salmi M, Auslender F, Bornert M, Fogli M. Apparent and effective mechanical properties of linear matrix – inclusion random composites: Improved bounds for the effective behavior. Int J Solids Struct 2012;49(10):1195–211.
[35] Fu S-Y, Feng X-Q, Lauke B, Mai Y-W. Effects of particle size, particle/matrix interface adhesion and particle loading on mechanical properties of particulate – polymer composites. Compos Part B: Eng 2008;39(6):933–61.
[36] Mori T, Tanaka K. Average stress in matrix and average elastic energy of materials with misfitting inclusions. Acta Metall 1973;21(5): 571–4.
[37] Segurado J, LLorca J. Computational micromechanics of composites: the effect of particle spatial distribution. Mech Mater 2006;38(8): 873–83.
[38] Chawla N, Ganesh V, Wunsch B. Three-dimensional (3D) microstructure visualization and finite element modeling of the mechanical behavior of SiC particle reinforced aluminum composites. Scripta Mater 2004;51(2):161–5.
[39] Ayyar A, Chawla N. Microstructure – based modeling of crack growth in particle reinforced composites. Compos Sci Technol 2006;66(13):1980–94.